Describing ion transport and water splitting in an electrodialysis stack with bipolar membranes by a 2-D model: Experimental validation

T. León [a,c,*], J. López [a,c], R. Torres [b], J. Grau [b], L. Jofre [b], J.-L. Cortina [a,c,d]

[a] Chemical Engineering Department, Escola d'Enginyeria de Barcelona Est (EEBE), Universitat Politecninca de Catalunya (UPC)-BarcelonaTech, Calle Eduard Maristany 10-14, Campus Diagonal Besòs, 08930, Barcelona, Spain
[b] Department of Fluid Mechanics, Escola d'Enginyeria de Barcelona Est (EEBE), Universitat Politecninca de Catalunya (UPC)-BarcelonaTech, Calle Eduard Maristany 10-14, Campus Diagonal Besòs, 08930, Barcelona, Spain
[c] Barcelona Research Center for Multiscale Science and Engineering, Campus Diagonal-Besòs, 08930, Barcelona, Spain
[d] Water Technology Center (Cetaqua), Carretera d'Esplugues, 75, 08940 Cornellà de Llobregat, Spain

ABSTRACT

Electrodialysis with bipolar membranes (EDBM) has drawn attention motivated by their application in generating reagents from salts. Due to the water splitting (WS) occurring at the junction of the bipolar membranes (BPMs), where the anion and cation layers are in strict contact, H+ and OH- are released from the BPM producing acid and alkali on the respective compartment. Considering this application, the interest of this work is to provide further understanding of the mechanisms of WS and transport of species in EDBM. This work develops and utilizes, for the first time, an experimentally validated two-dimensional (2-D) computational model, in which the Navier-Stokes and Nernst-Planck equations are coupled with the description of WS given by the Second Wien effect. In addition, a 1-D geometry is also proposed to perform a comparison between electroneutrality and Poisson charge conservation. The model is computationally solved using COMSOL Multiphysics. According to simulations, electroneutrality is valid for 2-D geometries. Moreover, the semipermeable characteristics of the membranes are assessed by means of evidencing a polarization effect resulting in a double-electric layer. The model proposed predicts a significant proton leakage, and facilitates the study of WS within the BPMs.

1. Introduction

Electrodialysis with bipolar membranes (EDBM) is one of the most rapidly progressing membrane-based methods for valorizing industrial wastes by converting salts into acids and alkalis [1–3]. Bipolar membranes (BPMs) are formed by two layers, one containing positively charged ionogenic functional groups (anionic) and one containing negatively charged ionogenic functional groups (cationic). Contrary to ion-exchange membranes (IEMs) commonly used in separation processes, the function of BPMs is the electro-dissociation of water [2]. Ideally, ions should not be transported across BPMs; some authors considered this assumption to simplify the mathematical models describing mass transfer across BPMs [4,5]. The objective of BPMs is to achieve water splitting in the junction of their layers (i.e., region in which the anionic and cationic layers are in direct contact), where water is dissociated into protons and hydroxyl ions without gases formation (e.

g., water disproportionation to $H_2(g)$ and $O_2(g)$) under the application of an external electric field. The resulting H^+ and OH^- exit the junction of the membrane, forming acid and base on the opposite side of the BPMs; a schematic view of an EDBM is shown in Fig. 2.

Over the past years, the application of EDBM has gained commercial interest mainly for its advantages in industrial applications. For example, Bunani et al. [6] reported a simultaneous separation and recovery of boron and lithium from aqueous solutions (lithium tetraborate at various concentrations, 34, 68, 170 and 340 mg/L) with applied voltages up to 35 V, and reaching a recovery efficiency up to 90%. Lately, EDBM has also been considered in the food industry. For instance, Tronc et al. [7] used EDBM to inhibit enzymatic browning in apple juice during storage, enhancing its color without changing its organoleptic properties. Moreover, integration of BPMs into electrochemical cells applying an electric field as the driving force for the migration of ions is an applicable method for acid and base generation from industrial liquid wastes [8–10]. As an example, Ibañez et al. [11]

Abbreviations

ED	electrodialysis
EDBM	electrodialysis with bipolar membranes
IEM	ion-exchange membrane
AEM	anionic-exchange membrane
CEM	cationic-exchange membrane
CFD	computational fluid dynamics
FEM	finite element method
EDL	electric double layer

reported production of NaOH and HCl solutions (up to 1 mol/L) from seawater reverse osmosis brines working under constant current densities (250–1000 A/m^2), and reaching current efficiencies in the range 60%–90%. The authors concluded that the production of acid and base becomes faster as the current density increases. The sodium concentration in the alkali channel after approximately 100 min reached 0.25 M when applying 250 A/m^2, while at 1000 A/m^2 it reached 0.85 M in a similar period of time [11]. In addition, the work described by Ibañez et al. [11] fits the circular economy principles, turning goods that are at the end of their service life into resources for other processes, and consequently resulting in closed loops within the industrial cycle [7,10].

Considering the numerous applications of EDBM, modelling their behavior has become crucial for understanding the distribution of electric potential and concentration over the membrane and adjacent cells, but also for scaling-up EDBM stacks. A great number of works are devoted to electrodialysis (ED) modelling, but only a few of them consider the effects of having BPMs. A summary of the most relevant research works on ED modelling using Computational Fluid Dynamics (CFD), are shown in Table 1. Apart from CFD analysis, other models found in literature [12–14] provided descriptions of ED systems with lumped or distributed parameters considering also the Nernst-Plank equations.

Among the recent publications on ED modelling, a notable work is the one recently presented by Kovalenko et al. [20]. The authors conducted computational simulations within the overlimiting current regime to analyze the effect of electroconvection in ED processes. Their research found that space charges of opposite sign are short-circuited at the membranes inside the channels, which result in a reduction of local current density. COMSOL Multiphysics [21] was utilized for the computations and focusing on nanometer-scale phenomena. In particular, their model considered very low concentrations of feed (salt) to facilitate computations.

The generation of protons and hydroxyls ions in the junction of BPMs

Table 1
Selected list of ED modelling efforts reported in the state of the art using CFD.

Model description	Specifications	Ref
2-D model involving the Nernst- Planck-Poisson-Navier-Stokes	Numerical simulations of ion and water transport involving electroconvection in an ED channel.	[15]
1-D model using Navier-Stokes & Nernst-Plank-Poisson	Desalination modeling of seawater and brackish water (multi-component solution).	[16]
1-D & 2-D models using Nernst-Plank-Poisson	Computational modeling of ion transport in continuous and batch ED.	[17]
1-D model using Navier-Stokes & Nernst-Plank-Poisson	Mathematical model of water splitting focus on the impact of the spatial distribution of fixed charges and catalyst at bipolar junction.	[18]
1-D models using Nernst-Plank-Poisson	Numerical simulation of ion transport for multi-component solutions.	[19]

is one of the most relevant features when modelling the physics phenomena involved. Based on published works, two modelling approaches for bipolar junction are typically considered [22,23]. The first approach assumes that the anion and cation layers are adjacent, therefore the distance between them is zero [23]. This null distance implies that the voltage and the concentration profile suffer a dramatic change in the bipolar junction. Moreover, in this virtually null distance (in the range of nanometers) the fixed charges are not compensated [22,24]. The second approach, instead, considers that there is a thin layer between the exchange-membranes, in which the charge is located [23,25]. Additionally, the influence of strong electric fields on the dissociation rate of weak electrolytes, described by the second Wien effect, must be considered [18,26]. Taking into consideration that the water molecule is a dipole, under the effect of a strong electric field, protons will be attracted to the cathode and hydroxyls to the anode. This phenomenon considerably accelerates the water dissociation ratio by several orders of magnitude, and consequently invalidates the Ohm's law [22]. Nevertheless, Parnamae et al. [24] question the second Wien effect as the sole cause of water dissociation. The authors stated that extremely high values of electric field at the junction of the bipolar membrane are required to achieve water dissociation. Additionally, the second Wien effect does not consider secondary effects associated with strong electric fields [27].

In this regard, this work presents a model for EDBM considering both flow and electrochemical equations, in which the second Wien effect accounting for water splitting is incorporated. Using COMSOL Multiphysics, simulations are performed in 1D and 2D domains to account for the concentration profiles of the salt (NaCl), acid (HCl) and base (NaOH) in the compartments. Additionally, the implications of Poisson and electroneutrality conditions in the simulations are discussed. Finally, the computational model is validated using data from EDBM laboratory experiments. Moreover, published works using CFD to describe the water splitting phenomena [22–26] are typically restricted to 1-D geometries. In this regard, to the best of the authors' knowledge, this paper presents for the first time a 2-D model at the centimeter-scale describing the water splitting and transfer of species by bipolar membranes.

2. Electrochemical flow physics modelling

2.1. Modelling assumptions

2.1.1. Fluid flow

When solving the equations to determine the velocity field, it is assumed that the Reynolds number is small enough to consider laminar flow, and the four solutions (feed, acid, base and electrolyte) are incompressible. Additionally, water transport through bipolar or monopolar membranes is not considered in the model limiting the number of influencing factors, and thus reducing the computation time. Water transport through the membranes occurs as a consequence of the water molecules consumed in the splitting of water. Although previous studies [22] reported that at low current densities the water transport is not a limiting process, the presence of water in the interfacial layer of the membranes is sufficient to produce H$^+$ and OH$^-$ even under a low current density. Moreover, the spacers are not considered in the mathematical model, as they will be considered in future work.

2.1.2. Electrochemistry

Several assumptions were made when solving the equations related to the transport of ionic species in the solution. It was assumed that the salt behaves as a strong electrolyte (i.e., no chemical equilibrium reactions in aqueous phase take place). Moreover, it was assumed that the solutions are ideal (i.e., activity coefficients are equal to 1). Additionally, membranes are considered to be ideal, i.e., the concentration of fixed charges in the membranes is uniform, and also highly selective, therefore cation exchange membranes only allow the transport of cations hindering the transport of anions. Conversely, anions are

transported across anion exchange membranes.

2.2. Equations of electrochemical flow motion

2.2.1. Hydrodynamics

The incompressible continuity and Navier-Stokes equations for an isothermal, Newtonian fluid determine the velocity and pressure distributions inside the channels [16,28].

$$\nabla \cdot \boldsymbol{u} = 0, \tag{1}$$

$$\rho \left(\frac{\partial u}{\partial t} + u \cdot \nabla u \right) = -\nabla p + \mu \nabla^2 \boldsymbol{u} + \rho \boldsymbol{f}, \tag{2}$$

where ρ is the density (kg/m^3), $\boldsymbol{u}$ is the velocity vector (m/s), p is the hydrodynamic pressure (Pa), μ is the dynamic viscosity (Pa·s), and $\boldsymbol{f}$ refers to body forces (N/kg).

The fluids inside the channels under a laminar regime describe a parabolic profile in channel with dimensions from $0 = x \leq W$, reaching the maximum values at the center of the channel. Eq. (3) describes this behavior [29].

$$u(x) = 3\overline{U} \left[1 - \left(\frac{x}{W} \right)^2 \right] \ at \ -1 \leq \frac{x}{W} \leq 1, \tag{3}$$

where u is velocity (m/s), $\overline{U}$ is the average velocity (m/s), x is the horizontal coordinate transversal to the channels (m), and W is the with of the channel (m).

2.2.2. Electrochemical transport of species

The flux of species is defined according to the Nernst-Planck equation, considering electric migration, diffusion and convection [13,24] as

$$j_i = -D_i \nabla c_i - z_i u_i F c_i \nabla \varphi + c_i \boldsymbol{u}, \tag{4}$$

where j_i is the molar flux (mol/(m^2·s)), D_i is the diffusion coefficient (m^2/s), c_i is the concentration (mol/m^3), z_i is the charge, and u_i is the mobility (mol·s/kg) of species i. F represents the Faraday's constant (96485 C/mol), and φ refers to the electrolyte potential.

The current density (i, A/m^2) can be obtained from Faraday's law by summing up all the contributions from molar fluxes multiplied by the species charges. Due to charge conservation, the convective term vanishes from Eq. (5) [16,28], resulting in

$$i = F \sum_{i=1}^{n} j_i z_i = F \sum_{i=1}^{n} (-D_i \nabla c_i - z_i u_i F c_i \nabla \varphi). \tag{5}$$

In order to determine species mobility, the Nernst-Einstein equation is utilized in the form

$$u_i = \frac{D_i}{RT}, \tag{6}$$

where R is the molar gas constant (8.314 J K/mol), and T is the temperature (K).

Additionally, the Donnan potential was used to account for charge discontinuities at the solution-membrane interface [16,28], which is written as

$$\varphi_s = \varphi_m + \frac{RT}{Z_i F} \ln \left(\frac{a_{i,m}}{a_{i,s}} \right), \tag{7}$$

where a_i is the ion activity (since ideality is assumed, activity is equal to concentration), and subscripts s and m refer to solution and membrane, respectively.

2.2.3. Charge conservation

Charge conservation in the solution can be established by using the electroneutrality condition (Eq. (8)), or the Poisson equation (Eq. (9)),

as [16,28].

$$\sum_{i=1}^{n} z_i c_i = 0, \tag{8}$$

$$\nabla^2 \varphi + \frac{F}{\varepsilon_0 \varepsilon_s} \sum_{i=1}^{n} z_i c_i = 0, \tag{9}$$

where ε_0 is the permittivity of the free space, and ε_s is the relative permittivity of the medium.

At the membranes, the charge conservation equation (Eq. (11)) incorporates a term related to the membrane charge, which corresponds to

$$z_x Q_x + \sum_{i=1}^{n} z_i c_i = 0, \tag{10}$$

$$\nabla^2 \varphi + \frac{F}{\varepsilon_0 \varepsilon_s} \left(z_x Q_x + \sum_{i=1}^{n} z_i c_i \right) = 0, \tag{11}$$

where z_x and Q_x are, respectively, the charge number and concentration of membrane fixed ions.

The non-linearity of the Poisson equation may induce numerical convergence complexities. At the macro-scale, the electroneutrality condition is suitable for charge conservation, but at relatively small domains (below Debye length) the mobile ions screen the electric fields [17] as

$$x_D = \sqrt{\frac{RT \varepsilon_0 \varepsilon_s}{F^2 I}}, \tag{12}$$

where x_D is the Debye length (m), and I is the ionic strength (mol/kg). The ionic strength reflects the effect of charges and interionic interactions on ionic activity coefficients written as [30].

$$I = \frac{1}{2} \sum C_i z_i^2. \tag{13}$$

The Debye length takes values in the order of 1 nm. Therefore, at this distance from the charged membrane the Poisson equation applies. However, at large distances, electroneutrality conditions can be applied [22].

2.2.4. Wien effect

In order to describe the effect of water splitting in the bipolar junction, the reaction is expressed by the following equilibrium expression [18,22].

$$H_2O \underset{r_w^+}{\overset{r_w^-}{\Leftarrow \Rightarrow}} \quad H^+ + OH^-, \tag{14}$$
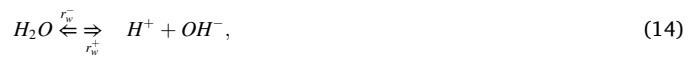
where r_w^+ and r_w^- are the reaction rates for forward and reverse reaction, respectively, described by

$$r_w^+ = k_w^+, \tag{14a}$$

$$r_w^- = k_w^- c_{H^+} c_{OH^-}, \tag{14b}$$

where k_w^+ and k_w^- are the forward and reverse rate constants. The ratio between k_w^+ and k_w^- represents the water dissociation constant [18,22].

$$K_w(298 \ K) = \frac{k_w^+}{k_w^-} = c_{H^+} c_{OH^-} = 10^{-14} \ kmol^2 \Big/ m^6. \tag{15}$$

Therefore, the overall rate of water splitting can be determined as [18,22].

$$r_w = r_w^+ - r_w^- = k_w^+ \left(1 - K_w^{-1} c_{H^+} c_{OH^-} \right). \tag{16}$$

A water molecule can be considered as a dipole. Under the application of an electric field, the positive part of the molecule (H$^+$) tends to

move towards the cathode, while the negative one (OH-) tends to be transported towards the anode. Consequently, electric fields accelerate water splitting, which is known as the Wien effect [18,22]. Onsager et al. [31] provided a quantitative description of this effect in the form

$$\frac{K_w(E)}{K_w(0)} = \frac{\Gamma_1\left(\sqrt{-2b}\right)}{\sqrt{-b}} = 1 + \frac{2^1}{1!2!}b^1 + \frac{2^2}{2!3!}b^2 + \frac{2^3}{3!4!}b^3 + \cdots,$$

$$b = A\frac{|E|}{\varepsilon_s\, T^2}\,, \tag{17}$$

where $K_w(E)$ and $K_w(0)$ are the ionic water products with and without the application of an electric field E, and $\Gamma_1(\sqrt{-2b})$ is the *Bessel function* of first order. For example, when the electric field strength E is in the order of 10^9 V/m (typical in a bipolar junction), the ratio $\frac{K_w(E)}{K_w(0)}$ changes from 10^4 to $10^{5.5}$ [18].

3. Model validation and assessment

3.1. Problem setup and computational approach

3.1.1. Computational Fluid Dynamics model

Considering the complexity of the partial differential equations that describe the EDBM process, this paper uses as a discrete mathematical approach based on the finite element method (FEM). The simulations presented in this paper are supported by the commercial FEM solver COMSOL Multiphysics 5.6. Simulations have been carried out using a platform HPE ProLiant DL560 Gen10 with 4 processors Intel Gold 6130 (16 cores/32 threads @ 2.10 GHz) resulting in a total of 64 cores/128 threads, 256 GB of RAM and a storage capacity of 8 TB HD.

3.1.2. Geometry

With the aim of simulating the EDBM process, 1-D and 2-D models were developed using COMSOL Multiphysics. Studying these two models allowed a comprehension of the mass transport and water splitting using different modelling approaches of charge conservation (i. e., Poisson and Electroneutrality). The models differ from each other, additionally to the number of dimensions, in their length. The 1-D model uses a length of 10 mm, whereas the 2-D model has a length of 200 mm. Although computations were made with a length of 200 mm, the charts and graphs presented in this work are displayed at 10 mm aiming to present results as little distorted as possible.

Regarding the 1-D model, two triplets of membranes were considered. The word triplet refers to the integration of an anionic, cationic and BPM [32]. The representation of channels and membranes is accomplished by stacking intervals one next to the other. Fig. 2 shows the 1-D geometry, the 2-D and 3-D models are displayed over it providing additional details of the representation of the membranes and channels given by the geometry.

The 2-D model also considers several ion-exchange membranes (anionic and cationic) resulting in two triplets of membranes. The representation of the BPM was accomplished by placing together an anodic and cationic membrane, with direct contact between each other. Consequently, the model involves a dilute channel, four concentrate channels (two acids and two alkalis), and two electrolyte channels; a modelled cell pair is shown in Fig. 1.

It is important to note that an EDBM experimental laboratory setup was used for validation of the computational model. Computations were contrasted against experimental data following the equivalent operational parameters. It is worth to mention that a periodic portion of the EDBM stack was the one simulated in 1-D and 2-D. The model simulates simultaneously the ion transfer phenomena and fluid dynamics within a periodic geometrical unit of the EDBM stack, as shown in Fig. 2. Using a small periodic tract of the stack means the reduction of the computational domain and consequently the reduction of the computational time. Gurreri et al. [33] used as well this periodic consideration in their
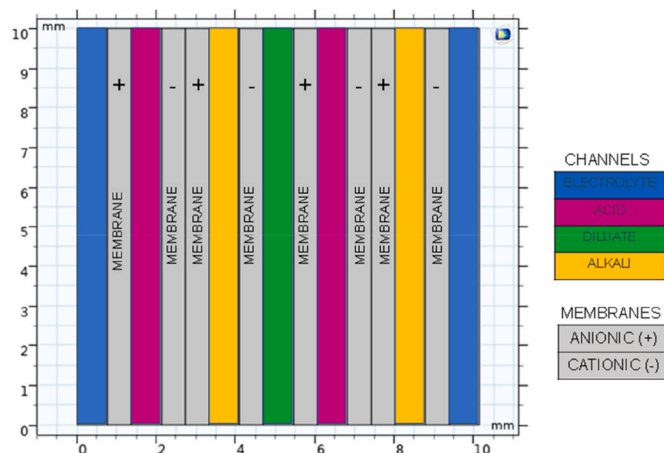

Fig. 1. Representation of the 2-D geometry: distribution of the ion-exchange membranes (cationic and anionic) and channels: acid (HCl), alkali (NaOH), electrolyte (Na$_2$SO$_4$), and diluate (NaCl) used for the computations.

work on reverse electrodialysis (RED) obtaining satisfactory results of the modelling of a RED cell. That being said, the periodic unit simulated in 1-D and 2-D contains 2 membrane triplets. Additionally, the channels and membranes are disposed symmetrically within the EDBM laboratory, in this sense the results obtained for these 2 triplets (i.e. periodic unit) are equivalent to the others. Fig. 2 schematizes the construction of the geometries contrasting the 1-D and 2-D geometries with the EDBM laboratory-unit (3-D).

3.1.3. Computational mesh

In order to solve the equations presented in Section 2 using a FEM approach, it is compulsory to discretize the flow field on a computational mesh, in which the values of the variables of the conservation equations (i.e., hydrodynamics, species, ion flux, charge conservation and Wien effect) are represented on the grid nodes. An accurate computational mesh must have high density of degrees of freedom in areas where the norm of the gradient of the variable is significant [34]. Given the geometry and symmetry of this model, it is recommended to refine the grid in the vicinity of the channel-membrane interface as shown in Fig. 3. Thus, the spatial distribution of grid points is concentrated in the boundary regions of the channels. In these regions, the description of mass transfer and charge transportation requires to be significantly accurate. With the intention of providing sufficient accuracy at efficient computational costs, the number of nodes in the 1-D model was 75000, whereas 266000 nodes were used in the 2-D model. The COMSOL option "Mapped" was the feature selected to build the mesh of the geometry. In detail, Fig. 3 shows the grid refinement at the channel-membrane interface, corresponding to the alkali-salt-acid channels. The mesh presented in Fig. 3 consists of 380000 elements and approximately $7 \cdot 10^6$ degrees of freedom.

3.1.4. Boundary conditions

The following boundary conditions have been considered:
Hydrodynamics: the flow was considered to be laminar and fully developed. Therefore, a time-averaged laminar velocity profile was used (Eq. 18). At the outlet of the compartments, it was assumed that the relative pressure was zero, and there was no return of the fluid. Additionally, for the membranes it was assumed no slip boundary conditions (Eq. 19). The effect of viscous stress was considered in the velocity profile.

Electrolyte potential: at the cathode, a potential of zero volts was assumed, while at the anode the potential was varied (Eq. 20–21).

Species and ion flux: the concentrations at the inlet were the same for all the simulations and are provided in Table 2 (Eq. 22). Additionally, at the outlet of the channels, flow convection drives the movement of fluid.
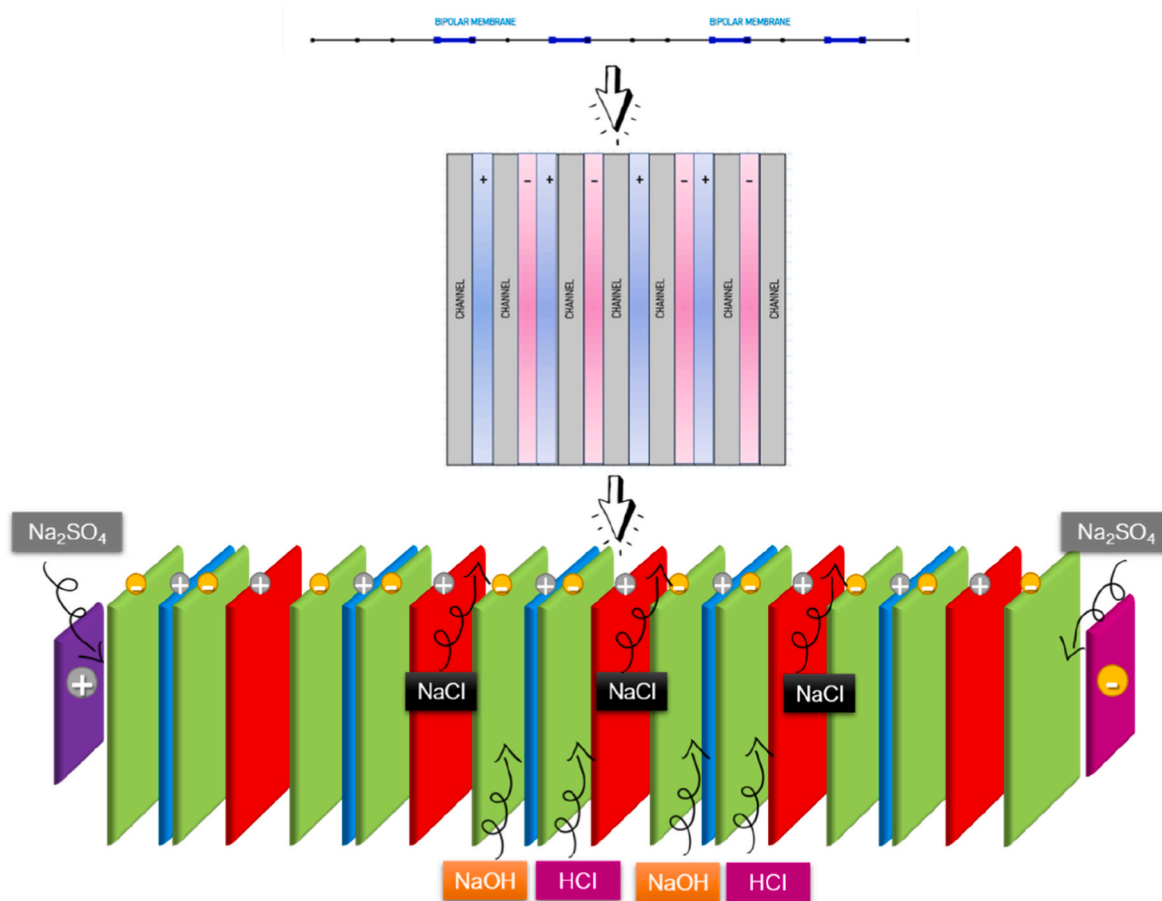
Fig. 2. Schematic representation (from 1D to 3D) of the scope of the simulation for the conversion of NaCl solutions onto NaOH and HCl.

The most relevant parameters for the study, such as initial concentrations and thicknesses of the membranes and channels, among others, are provided in Table 3. The value of the Stagnant diffusion layer thickness and the electrolyte relative permittivity were taken from the literature [35].

### 3.2. Experimental validation of the EDBM CFD model

The results obtained in the simulation were validated with experimental data obtained from an EDBM laboratory unit (BED1-4 with ED64004 and PC Fronted, PCCell). Fig. 4 shows the schematics of this unit. The electrical field was supplied using a direct current power supply (HCS-3202, Manson) with a maximum capacity of 15 A. The EDBM cell has four loops of solutions: acid, base, salt and electrolyte. The cell comes along with four centrifugal pumps, which push the fluids from the vessels to the membranes and back to them in a closed-loop configuration. The EDBM setup is equipped with some sensors in order to measure several parameters such as conductivity and temperature.

Experiments were carried out at a constant applied voltage of 5 V, which is equal to the voltage simulated in the computational model. The initial concentration of acid (HCl) and base (NaOH) solutions were 0.05 mol/L. On the other hand, the initial concentration for the salt solution was 2 mol/L NaCl. The initial volume in the acid and base tanks were 1 L, while for the salt tank was 1.5 L. Five triplets of commercial ion exchange membranes with a transversal area of 0.028 m^2 were part of the EDBM unit used in the experimental validation. The membranes tested in this paper were AR103 N (anionic), CR61 N (cationic), and AR103N-t (anionic treated to be used as bipolar) from the manufacturer SUEZ-WTS. Characteristics and features of the membranes tested are

detailed in Table 4. The velocity inside the channels was 7 cm/s, resulting in a flow rate of 50 L/h 5 mL samples were taken directly from the tanks every 5 min. For all the experiments, several operational parameters such as voltage, volume evolution, conductivity, etc. Were controlled. Experiments stopped when the conductivity of the salt, base and acid reached a plateau. For what is known, the conductivity of the salt decreases as a result of ion transfer, at the same time the acid and base increase their conductivity due to ion gain and water splitting [8, 36]. However, after some time the concentration gradient in the compartments may result in a back-ion diffusion. To avoid this problem, experiments have to stop when the values of conductivity do not increase or decrease, respectively. Lee et al. [37] stated in his work that the conductivity was proportional to the salt concentration. At low concentrations, however, non-idealities should be considered due to decrease in the molar electrical conductivity of the salt. Considering these observations, the evolution of conductivity was monitored during the EDBM operation (data not shown).

Previous experiments carried out with this type of membranes concluded that the ideal operational time was within 4–5 h [9]. For the purposes of this research, and aiming to optimize the calculation time, the operation time has been set to 1 h; this operation time has been fixed for the experimental procedure and the CFD computations.

In order to determine the concentrations of the species in the samples, different analytical procedures have been followed. All the samples have been analyzed by ion chromatography (Dionex ICS-1000 and ICS-1100) with the cation-exchange IONPAC® CS16 anion-exchange IONPAC® AS23 columns. The mobile phase was 30 mmol/L CH_3SO_3H for the cation-exchange column, and a mixture of 45 mmol/L Na_2CO_3 and 0.8 mmol/L $NaHCO_3$ as eluent solution. In relation to the concentration of acid and base, they were analyzed by titration using an automatic
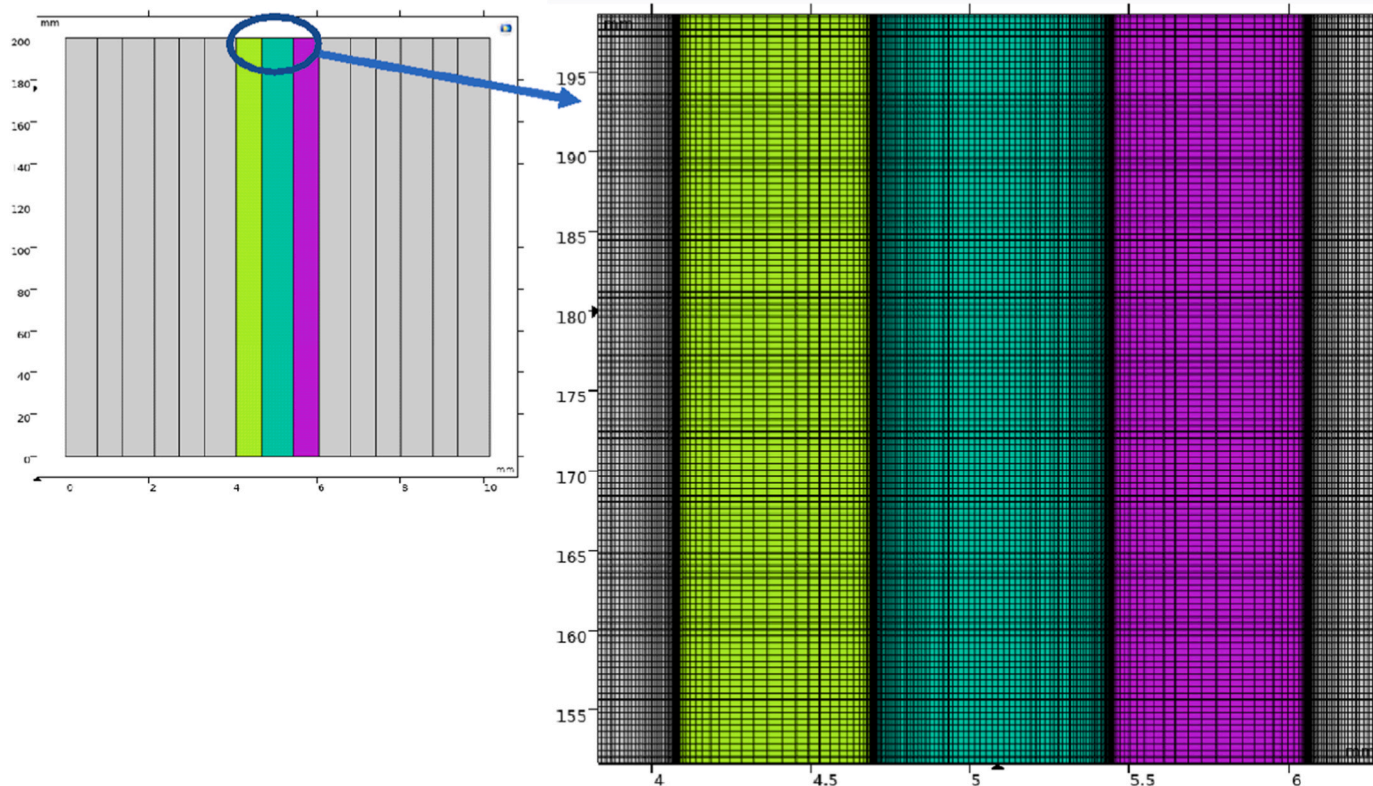
Fig. 3. Spatial discretization (mesh) in a section of the 2-D model. The color representation equivalates to the following: a) light green represents a cationic membrane, b) dark green represents the diluate compartment, and c) purple represents the anionic membrane. (For interpretation of the references to color in this figure legend, the reader is referred to the Web version of this article).

Table 2
Boundary conditions considered in the EDBM simulations.

Condition	Description	Equation
$y = 0$	$v_x = 0; v_y = u_0$	(Eq. 18)
	$v_x = 0; v_y = 0$	(Eq. 19)
$x = 0$	$\varphi(0, y) = 0$	(Eq. 20)
$x = L_{stack}$	$\varphi(L_{stack}, y) = \Delta\varphi$	(Eq. 21)
$y = 0$	$c(x, 0) = c_0$	(Eq. 22)
$y = L$	$D_i \dfrac{\partial c_i}{\partial y} = 0$	(Eq. 23)

Table 3
Parameters employed in the simulations of the EDBM.

Name	Value	Description
A	0.09636 s^3·A·K^2/(kg·m)	Wien effect coefficient (Onsager relation)
Q_x	1000 mol/m^3	Concentration of membrane fixed ions
c0	2000 mol/m^3	Salt initial concentration
c1	50 mol/m^3	Base/acid initial concentration
D_{Cl^-}	2.03·10^{-9} m^2/s[1]	Diffusion coefficient of Cl$^-$
D_{H^+}	9.312·10^{-9} m^2/s[1]	Diffusion coefficient of H$^+$
D_{Na^+}	1.334·10^{-9} m^2/s[1]	Diffusion coefficient of Na$^+$
D_{OH^-}	5.26·10^{-9} m^2/s[1]	Diffusion coefficient of OH$^-$
u_0	7 cm/s	Velocity inside the channels
ε_0	8.85· 10^{-12} (F/m)	Relative permittivity of the free space
ε_r	78	Electrolyte relative permittivity
K_w	10^{-14} kmol^2/m^{6a}	Water dissociation constant at zero field
k_w^-	1.3·10^8 m^3/(s·mol)^a	Reverse rate constant, water dissociation
L_{mem}	6·10^{-4} m	Membrane thickness
L_{sdl}	7.62·10^{-4} m	Stagnant diffusion layer thickness
T	298.15 K	Temperature

[a] Values reported are at 298.15 K.
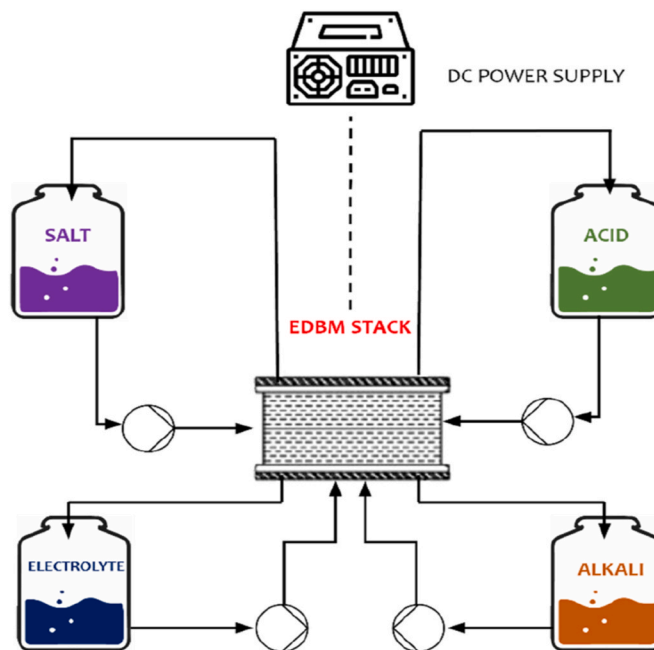
Fig. 4. EDBM laboratory setup scheme based on a closed-loop configuration with four independent vessels: i) acid (HCl), ii) alkali (NaOH), iii) electrolyte (Na$_2$SO$_4$), and salt (NaCl).

titrator (T70, Mettler Toledo) equipped with an automated carousel-type titration stand (Rondolino, Mettler Toledo). HCl 0.01 M and NaOH 0.01 M (previously standardized) were used for titrating basic and

Table 4
Characteristics ion-exchange membrane used in the experimental validation.

Manufacture	Membrane	Identification	Functional groups	Ion Exchange Capacity	Thickness (µm)	Composition	Permselectivity (%)	Refs.
SUEZ WTS	AEM	AR103 N	quaternary ammonium	2.37 (meq/dry g resin)	300	Woven polypropylene	92	[38]
	CEM	CR61	sulfonic acid	2.2 (meq/dry g resin)	300		95	
	AEM- treated	AR103 N tr.	quaternary ammonium	2.37 (meq/dry g resin)	300		92	

acidic samples, respectively.

4. Results and discussion

EDBM is particularly different from conventional ED due to the phenomena of water splitting occurring at the junction of the BPMs. Considering this particular characteristic, analyzing the species migration and the generation of protons and hydroxides are the main focus of study in this work. In particular, this paper presents computations and analysis of four species: Na^+, Cl^-, H^+ and OH^-. One of the most important parameters when describing the transfer phenomena encountered in EDBM is the charge conservation approximation. Aiming to understand the H^+ and OH^- generation, the charge conservation must be defined. Historically, electroneutrality has been the most common choice in electrochemical models, due to the small absolute values for the permittivity of typical solvents [39]. Considering the length (200 mm) of the 2-D model presented in this paper, electroneutrality becomes a plausible approximation since the Debye length (i.e., where neutrality conservation is neglected) is typically of the order of nanometers [40]; this would be a crude approximation for the purpose of this work. On the contrary, the low computational cost of the 1-D model allows the integration of the Poisson equation on a very fine mesh. Results of both 1-D and 2-D models are presented and discussed in the following sections. The water splitting is analyzed by means of the concentration profile of protons and hydroxides. Furthermore, the results from the CFD simulations are contrasted against experimental data obtained from an EDBM experimental laboratory unit.

4.1. EDBM model resolution: 1D comparison between electroneutrality and Poisson

In order to compare between electroneutrality and Poisson approximations in a 1D-model with four interacting species (Na^+, Cl^-, H^+ and OH^-), some considerations were made. The H^+ and OH^- initial concentrations were related to the dissociation rate of the water; while the Na^+ and Cl^- initial concentrations were expressed in the frame of the electroneutrality principle ($\sum_{i=1}^{n} z_i c_i = 0$). Therefore, the concentration value of one species is calculated from the others based on the electroneutrality condition. On the other hand, the Poisson approximation enables to define different values for Na^+ and Cl^- initial concentrations as the electroneutrality does not need to be conserved in the system ($\sum_{i=1}^{n} z_i c_i \neq 0$). However, in order to compare both the electroneutrality and Poisson computations, the initial concentration of NaCl was set to 2 M. Focusing on the comparison of the charge conservation approximations in the 1D model, Fig. 5 presents several graphs: (a) Na^+ concentration profile, (b) H^+/OH^- concentration profile, and (c) electrolyte potential evolution along the length of the EDBM unit.

Fig. 5a illustrates the Na^+ concentration profile at constant voltage of 15 V. The concentration increases and decreases responding to the
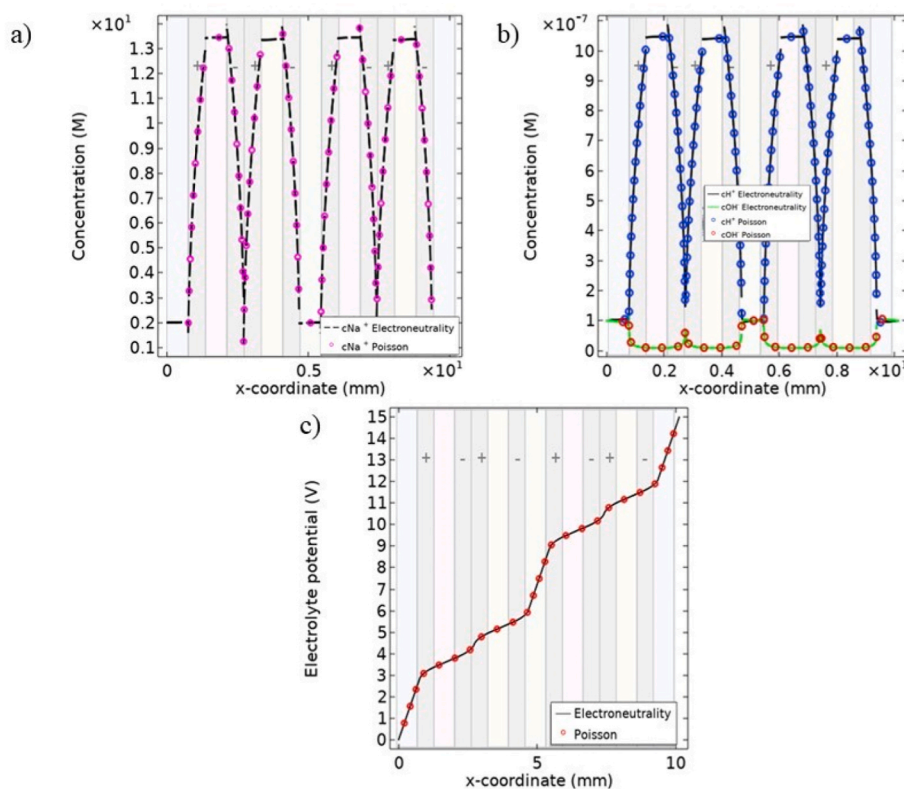
Fig. 5. Results from the 1-D geometry in terms of a) Na^+ concentration profile, b) H^+ and OH^- concentration profile, and c) electrolyte potential evolution at 15 V by applying electroneutrality and Poisson charge conservation along the x-coordinate (mm).

nature of the membranes, either with a positive (anion exchange membrane) or negative (cation exchange membrane) charge. Concentration profiles at the boundary of the membrane-solution are explained by the Donnan potential effect near the surfaces. Fig. 5a also contrasts the correspondence between electroneutrality and Poisson approximation through the comparison of the Na^+ concentration profile across the length of the system. It can be seen that the results from electroneutrality and Poisson overlap. Additionally, it can be noted that for the 1-D one presented in this paper, both numerical solutions converge and are valid to study the EDBM transfer phenomena.

Fig. 5b presents the H^+ and OH^- profile concentration evidencing the water splitting phenomena. At the junction of the bipolar membranes, the behavior followed by the H^+ and OH^- is coherent with the charge of the two ion-layers that form the bipolar membrane. The proton concentration decreases in the anion-layer and increases in the cation one. A 1-D geometry is still not sufficient to describe a detailed water splitting at the bipolar junction. However, it demonstrates the second Wien effect resulting in the production of protons and hydroxides when using bipolar membranes.

The electrolyte potential is illustrated in Fig. 5c for both electroneutrality and Poisson approximations. The profiles mostly overlap, which may support that any of these charge approximations are suitable to simulate the EDBM process. One important point observed in Fig. 5c is the presence of humps at the membrane boundary, evidencing the Donnan potential effect.

Considering the results from the 1-D model, it can be concluded that different charge conservation approximations have no significant effect on the concentration distribution, or the electrolyte potential, in the 1-D EDBM model. Some previously published papers agree on the superposition of electroneutrality and Poisson approximations. Volgin and Davydov [41] analyzed the ion transport through ion-exchange and bipolar membranes and adjacent diffusion layers using Nernst–Planck and Poisson (NPP) equations considering the effect of space charge. They found that at the zone adjacent to the outer boundary of the diffusion layer, the electroneutrality and Poisson approximations are equivalent. Moreover, Strathmann et al. [25] in their research work on limiting current density highlighted the agreement between Poisson and electroneutrality in all the regions except for the space charge. However, both Volgin and Davydov [41] and Strathmann et al. [25] agree that electroneutrality is disturbed due the variation in the count of counter-ions and co-ions at the region where the anion and cation-exchange layers meet. This work presents evidence of the validation of the compatibility of Poisson and electroneutrality approximations. These statements encourage the application of electroneutrality approximation in the 2-D model.

4.2. EDBM model resolution: 2D with electroneutrality

A 2-D model warrants a wider understanding of the phenomena occurring in the EDBM process. Within this framework, choosing the proper charge conservation approximation is crucial. Results from the 1-D model corroborated that conducting simulations adopting electroneutrality is a valid consideration. The dimensions of the 2-D model proposed in this paper are much greater than the typical Debye length (i. e., where electroneutrality becomes invalid) [40,42]. Given what has been described, both in the junction of bipolar membranes and through the ion-exchange membranes, electroneutrality must be conserved. An additional important point to highlight is the fact that the 1-D geometry presented in this paper does not consider convection effects in the model, while the 2-D allowed to visualize the evolution in the profile concentrations and velocity distribution. By means of using a more complex geometry— 2-D model, a deeper analysis of the EDBM process can be made.

4.2.1. Velocity distribution in the channels

The velocity distribution in the channels is illustrated in Fig. 6. The velocity profile is shown along the streamwise y-direction in the areas corresponding to the acid-base-salt and electrolyte solutions, as the membranes are assumed to be impermeable to the solutions. The solutions flow through the inner side of the channels with the velocity decreasing to zero at the boundaries. This profile was the expected one for a laminar regime [28]. To confirm this statement, the Reynolds number was calculated, Re = 105.24; this value considered: i) diameter of the pipes of 7 mm, ii) velocity inside the channels: 7 cm/s, and iii) viscosity and density of the fluids at 20°. According to Ryan et Johnson [43] this value of Reynolds (105.24) was way below the critical value to describe a turbulent flow. Certainly, at this small Reynolds number, the flow is described as laminar and is being dominated by viscosity. Velocity profiles for fully developed flow, such as the one considered here, describes a parabolic shape as shown in Fig. 6. The friction at the walls of the channels slows the fluid down, consequently at the membrane surface the fluid's velocity is zero. Moving away from the wall the velocity of the fluid increases, and reaches a maximum at the center of the channel. The velocity function describing the.

4.2.2. Concentration profiles

Fig. 7 shows the concentration profiles in color-scale at different positions within the EDBM stack. The concentration profiles are presented at a) the salt (diluate) channel and the alkali-acid adjacent channels, and b) the junction of one of the bipolar membranes. It has to be mentioned that the concentration profiles were obtained in a stationary regime. The initial concentration in the different channels differs
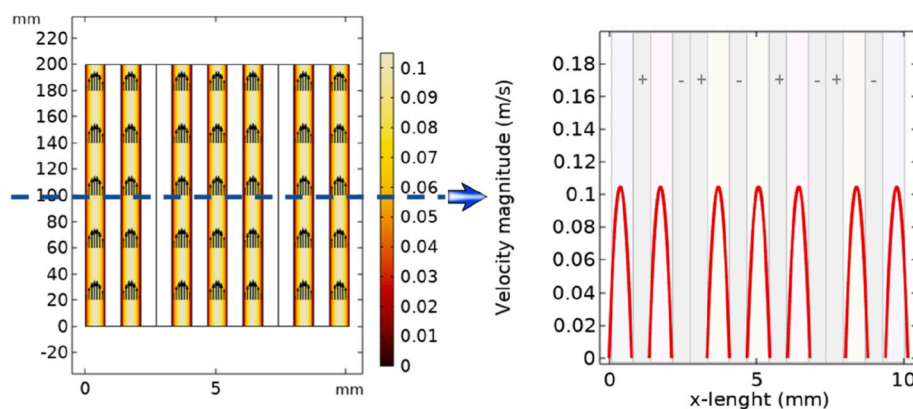

Fig. 6. Velocity profile (m/s) in the channels along the EDBM stack for the 2-D geometry. At the left side of Fig. 6 the velocity distribution within the channels is shown using a color legend; the light yellow in the middle of the channels equivalates to values of velocity in the range 0.09 to 0.07 m/s, while the dark red equals to velocities close to zero. (For interpretation of the references to color in this figure legend, the reader is referred to the Web version of this article).
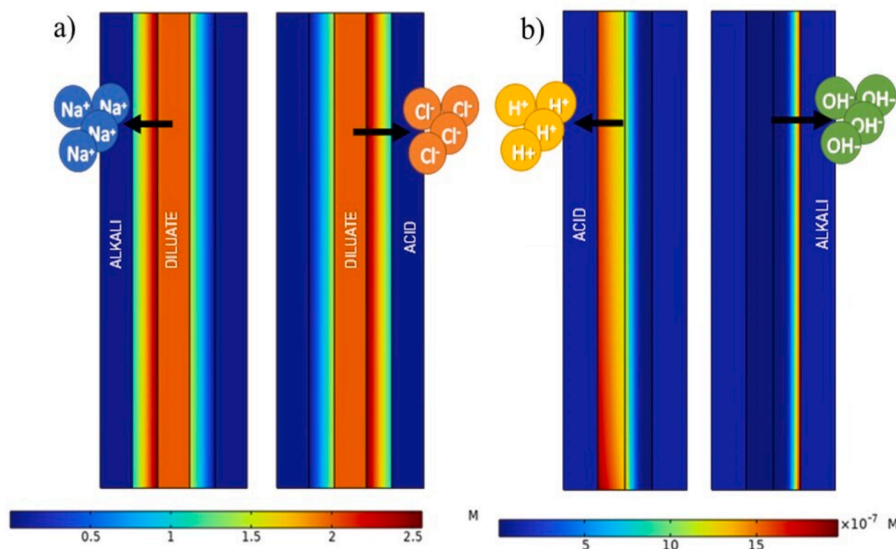
Fig. 7. Concentration profiles along the EDBM stack at 5 V from the 2-D geometry a) at the dilute and alkali-acid adjacent channels for NaCl, and b) at the interface of one of the bipolar membranes and the adjacent channels.

from zero; this consideration was made with the intention of favoring the transport of charged species. It is observed that the ion concentration tends to increase in the regions adjacent to the anionic and cationic membranes.

Focusing on Fig. 7a, the Donnan exclusion should be mentioned; it causes the favored transport of charged species according to the nature of the ion-exchange membrane. The concentration of sodium increases in the region adjacent to the cationic membrane (left side of the dilute channel), while it decreases at the opposite side, proving the semi-permeability characteristic of the membrane. Likewise, the concentration of chloride ions intensifies next to the anionic membrane (right side of the dilate channel).

As a consequence of the electroneutrality condition, the charges must be compensated at all times. Fig. 7a evidences this condition, apparently there is an equimolar flux of Na^+ and Cl^- to the alkali and acid channel compartment. Considering in detail Fig. 7b, the water splitting phenomena can be clearly observed by means of the flux of protons and hydroxides from the junction of the bipolar membrane. The flux of H^+ and OH^- from the bipolar membranes will increase the acidity and basicity in the adjacent channels. However, looking at the results in Fig. 7b, the flux of protons is considerably different from the hydroxide flux. This divergence can be attributed to the different ionic mobility of these species. Protons have a much higher ionic mobility due to their hydrogen bonding [44], resulting in protons moving faster than hydroxides to the adjacent channels. With this in mind, it can be intuited that the acid concentration will be lower than the one of base due to the proton leakage to other compartments. The proton leakage has been previously observed experimentally in the literature [19,45]. Kuldeep et al. [19], using a 1-D model in COMSOL Multiphysics and experimental data observed ion leakage through the ion exchange membranes. The authors reported a major leakage of protons to the concentrate compartment compared to the one of hydroxyls. They attributed this to the smaller size and high mobility of the proton [19]. Likewise, Ran et al. [45] referred to acid recovery through diffusion dialysis. Their research work highlighted the retention of metal cations and the spontaneously permeate of anions through the anion exchange membrane. However, the protons did not behave accordingly; a proton-leakage to the concentrate compartment was a result of their higher mobility (as compared to the metal cations).

Reconsidering Fig. 7b, the flux of protons and hydroxides coming from the junction of the bipolar membrane evidences the water splitting

phenomena associated with them. The water splitting in bipolar membranes responds to two effects: i) the strong electric field (i.e., the second Wien effect), and ii) the proton transfer reaction occurring between the functional groups of the membranes and water [18]. Fig. 7b shows how the generated protons and hydroxides flow through the cation and anion exchange membrane of the BPM, respectively. Moreover, Fig. 7b evidences that the reaction of water splitting occurs in a thin layer at the junction of the bipolar membrane. Moreover, the effect of the electrical field must be also considered in the discussion. The cations are attracted to the cathode, therefore the protons flow to it. When the protons reach the anion-exchange membrane (AEM) attracted by its charge, the protons are retained in the acid compartment. Likewise, the hydroxyls flow to the anode and are retained in the base compartment.

In order to obtain a deeper understanding of the EDBM operation, several graphs (Fig. 8) were prepared to help understand how this model interprets the flux of ions coming from the BPMs junction and also through the channels at 10 mm length and 5 V.

Fig. 8a presents the profiles of protons and hydroxyls along the EDBM unit length. The semi-permeable characteristic of the ion-exchange membranes are once more demonstrated. The concentration of H^+ increased at the cation membrane regions, likewise the OH^- concentration raised at the anion membrane regions. Focusing on Fig. 8a, it is evident that the values of concentration of OH^- are greater than the one of H^+. At the interval of the arc length $4 < x < 6$ (i.e., the diluate compartment and the adjacent membranes) the concentration of H^+ reached 8×10^{-7} M while the OH^- reached 16×10^{-7}. This significant difference is attributed to the different mobility of the species. The higher mobility of the protons allows them to move faster resulting in leakage to the other compartments. As a result, the concentration of protons is expected to be lower; these considerations were already mentioned in the color-scale graphs analysis. The leakage of protons was reported several times in the literature. For instance, Al-Dhubhani et al. [3] tested five commercial membranes and pointed out that a low current efficiency is linked to low selectivity of the AEM associated with proton leakage. From the five commercial membranes, the ones from the manufacturer Yichen had the most considerable proton leakage (i.e., the lowest efficiency). The authors also recommended the use of proton blocker membranes to enhance the selectivity of the AEM and reducing the H^+ leakage.

It is worth to mention that several authors have designed methods to quantify experimentally the proton leakage, thus realizing the
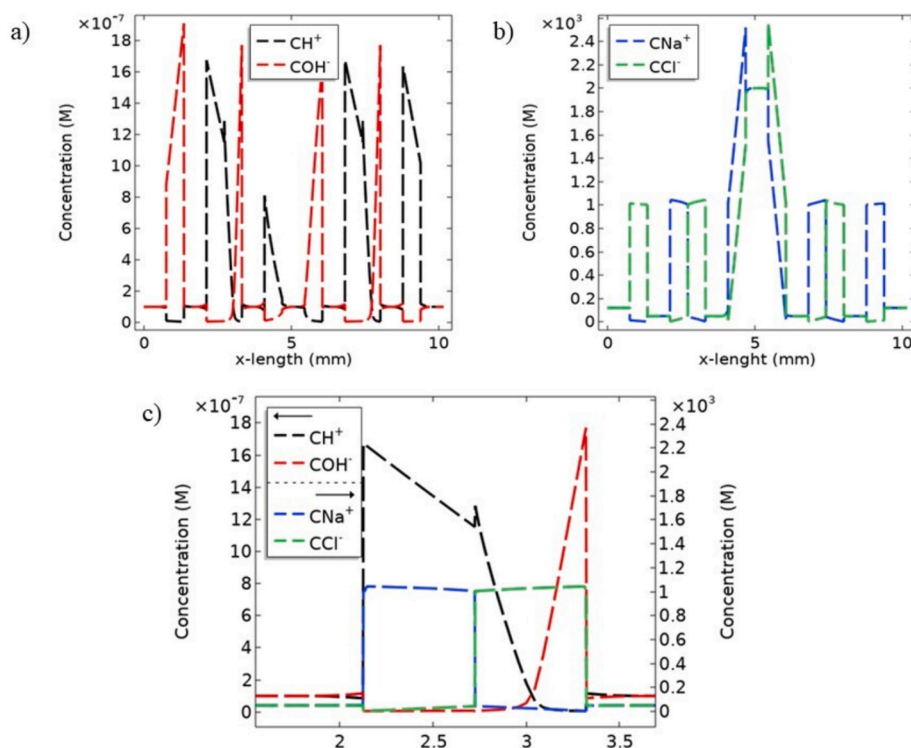
Fig. 8. Concentration profiles from the 2-D geometry a) H$^+$ and OH$^-$ profile concentration at 10 mm arc length, b) Na$^+$ and Cl$^-$ profile concentration at 10 mm arc length and c) ion concentration profile at the BPM at 5 V along the x-coordinate (mm).

importance of this phenomena in the EDBM performance. Lorrain et al. [46] proposed a method using platinized-titanium electrodes to measure the leakage through anion-exchange membranes. They also verified this estimation by calculating the associated transport numbers. Raucq et al. [47] proposed as well a method using platine-coated titanium electrode and evaluating the effect of the proton leakage on the current efficiency.

Fig. 8b exposes the profile concentration of Na$^+$ and Cl$^-$ throughout the stack at 10 cm length. Looking at the profile evolution, several inferences can be made about it. First, the evidence of polarization is observed at the membrane's surfaces, showing the accumulation of species in the solution at the vicinities of the membrane. Abrupt changes at the membrane interface results in a small region (viz. Debye length). At Debye length the neutralization takes place due to the action of the counterions with the fixed charges of the membranes; as a result, the concentration of the fixed charges is much higher [24]. At the interface of the base channel-cation exchange layer (i.e., arc length = 4 cm) the concentration of chloride increased, suggesting an accumulation of the negatively charged species, which is related to the accumulation of the rejected anions nearby the membrane layer. Moreover, it can be observed that, for example, the concentration of Na$^+$ (or Cl$^-$) increased to 2500 mol/m^3 in the membrane side at the interface cation (or anion) exchange membrane – solution. This sharp change at the interface of the membrane-solution resulted in an electrical double layer (EDL). An EDL forms when two conducting phases converge at an interface [48]; one phase is attributed to the charge of the membrane while the other is related to the electric field applied to the system. Fig. 8b evidences the stated before showing jumps in the concentration evolution of Na$^+$ and Cl$^-$.

Additionally, a detail of concentrations at the BPM is presented in Fig. 8c. Due to the fact that NaCl presented a higher concentration in solution, the anion layer in the BPM must be initially saturated with Na$^+$, correspondingly the cation layer will contain Cl$^-$. All these assumptions were made based on the fact that a stationary regime was considered for the simulations. Similar profiles at the BPM were presented by Mareev et al. [18], who reported that NaCl compensated the

fixed charges at the BPM. Additionally, in the simulations it was observed that some co-ions could be present at the layers of the BPM, i. e., Na$^+$ and Cl$^-$ at the anion and cation layer of the BPM, respectively. This can be related to a diffusion phenomenon from the solution to both layers. This has been previously reported by Vermaas et al. [49], who studied the transport of ion cross-over across a Fumatech BPM, observing that up to 10% of Na$^+$ and 9% of Cl$^-$ could permeate.

4.2.3. Electrolyte potential analysis

Fig. 9 shows the distribution of the electric potential along the membrane stack at different values of external voltages (2V–16V). The
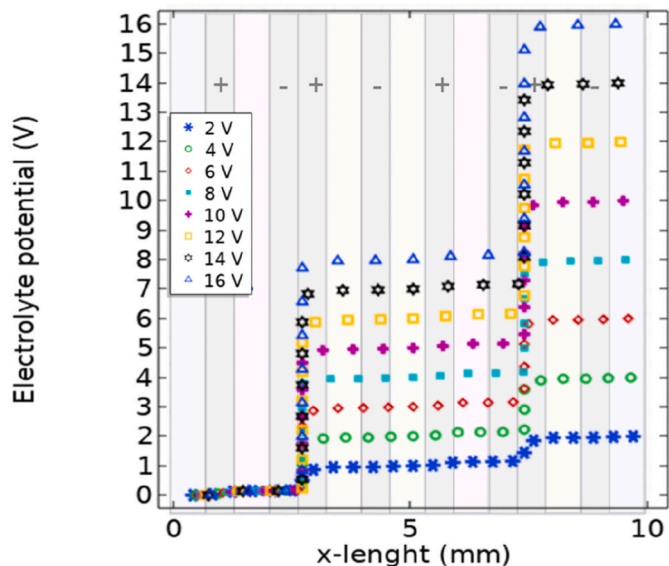

Fig. 9. Distribution of the electrical potential along the 2-D geometry at 2 V,4 V,6 V, 8 V,10 V,12 V, 14 V,16 along the x-coordinate (mm).

electric potential evolves proportionately for all the values of external voltages, increasing dramatically at the bipolar junction (i.e., where the anion and cation exchange layer are in strict contact), but for the rest of the geometry the electric potential describes a stable behavior. These dramatic changes can be attributed to ohmic losses at the interface of the BPMs. This depletion occurs to compensate for the difference in Donnan potential coming from arising concentration polarization [50]. Ramírez et al. [42] in their work on current-voltages curves of BPMs highlighted the fact that the water splitting effect was dominant in the evolution of electrical potential. The research of this work agrees with the results presented in that work.

Considering an ideal behavior of an EDBM unit, the overall electrical resistance is the sum of the resistances given by the membranes and the solutions. However, polarization happening due mass transfer in the system may invalidate this condition resulting in non-Ohmic resistance conditions within the EDBM units. The limiting current curves (not shown) describe this behavior in three regions: i) ohmic, ii) limit, iii) overlimiting [25]. In the first region the curve current density-voltage describes a linear behavior, when the limit current is reached the curve describes a non-linear trend and consequently a voltage drop is reported at the limiting region (i.e., non-Ohmic region). This deviation is due to the polarization phenomena happening at the membrane interface; this fluctuation has already been reported several times in this paper.

4.3. Experimental validation of the CFD model

This section presents the validation of the CFD model proposed in this paper against experimental data. As it was stated in previous sections, the comparison was made against laboratory results provided by an EDBM unit. Some considerations were kept equivalent in both experiments and simulations, such as: i) initial conditions and operational parameters (e.g. velocity inside the channels, and concentrations, among others), ii) EDBM configuration (i.e., the position of membranes and consequent channels), and iii) time operation taking in consideration the values of conductivity in the experimental results. One important difference to highlight in this discussion is that the results from the CFD model are stationary in time, whereas the data from the experiments are time dependent. However, the CFD model provided small-scale information at particular regions of the domain that were unattainable in the experiments. In this regard, the information from the CFD simulations facilitates to better understand the phenomena governing the main processes in EDBM. In this regard, future investigations will focus on performing time-dependent computations to further assess the similarities and differences between the CFD model and laboratory experiments.

To compare the stationary CFD results to the time-dependent experimental data, several factors correlating the length of the stack with the operational time were introduced. In particular, the following assumptions have been made. First, as the EDBM laboratory setup works in a closed-loop regime, the solutions are constantly flowing from the EDBM stack to the tanks and vice versa. Experimentally, considering the velocity inside the channels, the time that the fluids require to pass through the EDBM unit [i.e., EDBM stack (x = 50 cm), pipes, wires and pumps] was estimated in 14.4 s. Thus, 60 min (i.e., the operational time) is equivalent to 250 flow through times in the EDBM set-up. Secondly, experimental dilution factors in the feed tank were incorporated in the estimation to account for concentration changes at the inlet of the feed solution along the experiment. Lastly, it must be noted that the geometry considered in this paper was 20 cm, while the total length of the stack is 50 cm. That being said, the concentration values at lengths larger than 20 cm were calculated from mathematical correlations that allowed to properly extrapolate the data.

It is important to mention the complexity that comes along with solving a 2-D geometry, and resulting in high computational costs. An operation time of 1 h at 5 V is short comparing to the average EDBM

operation conditions [8,11,51]. Such low inputs voltage simplified the computations reducing the computation time from 7.27 h at 17 V to 1.5 h at 5 V. Higher values of electric fields leads to very large concentration gradients, and consequently a more refined grid is required. Moreover, at the higher values of inputs voltage—, current the water transport to the interfacial layer becomes relevant [22]. For the sake of optimizing the computational costs, the experimental validation presented in this paper is justified at an operation time of 1 h at 5 V. Considering all this, Fig. 10 presents the comparison between the CFD model against the experimental results for the profile concentration for the acid and the alkali solutions.

The experimental results plotted in Fig. 10 were obtained through the analytical technique of automatic titration. The values of concentration of the base and acid solution seem to be dispersed; the experimental results were still not stable enough to show a consistent behavior in the profile evolution after 1 h. Commonly, EDBM experiments take from 4 h to 40 h to reach the plateau in concentration, as pointed out by different authors [8,11,51]. This operation time varies according to the inner features of the membranes. However, as stated before, the operation time was set to one 1 achieving a reduction in the calculation time of the model. Herrero-Gonzalez et al. [8] reported an EDBM operational time of 40 h in their study of the production of highly concentrated acid and alkalis. In the first hour the authors reported a dispersed distribution of the values of Na^+ and Cl^- concentration. The ion concentration in this first period (i.e., t < 1 h) of time fluctuated constantly. After 1 h, the ions flux became smooth, and consequently the ion concentration started to describe a defined growing trend [8]. Analyzing the experimental results from this paper, it was evident that in 1 h (i.e., operational time) the concentration of the ionic species was still varying and had not reached a stable behavior. The acid concentration at 30 min was 0.073 M, after 5 min decreased to 0.0645 M, but at 40 min increased again to 0.08 M. This fluctuation agrees with the experimental results presented by Herrero-Gonzalez et al. [8].

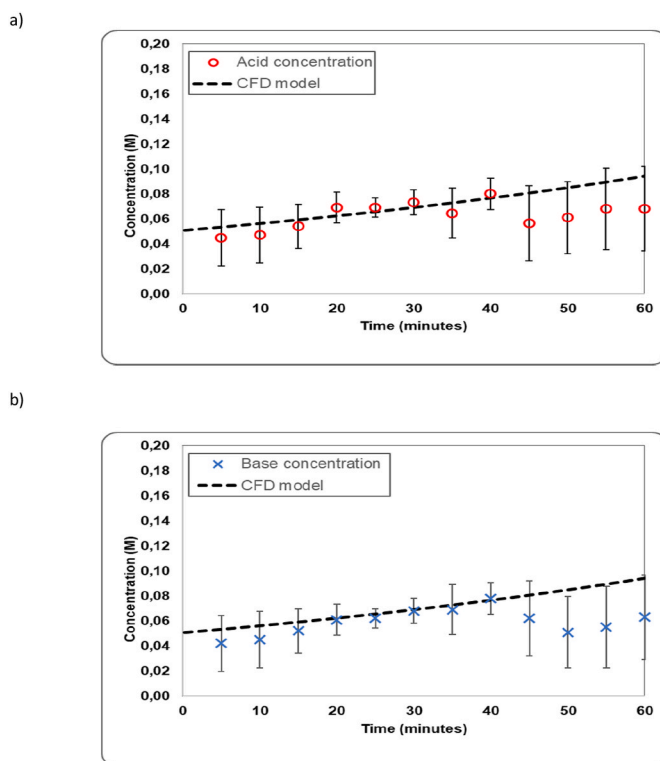Contrasting the experimental data with the CFD model several

Fig. 10. Comparison between experimental concentration profiles and results from this CFD model for a) Acid and b) Alkali.

interpretations are made around this comparison: i) although the experimental data was dispersed during the operation time, most of the error bars associated with it intersect the data from the model. This implied a good agreement between the simulated and experimental profile concentration values; and ii) the operation time of 1 h was not long enough to visualize a defined tendency in the results. As explained in literature [10,52], the ion evolution was faster in the first period of time, but as time passed by, the resistance of the stack increased. With the increase of the resistance, the variation in the concentration was less pronounced after the first hour of operation. Therefore, it is suggested to perform the computation and experiments for extended periods of time to have a deeper comprehension of the ion evolution in the EDBM process.

5. Conclusions

Computational 1D (10 mm) and 2D (200 mm) models have been developed to describe the transport species and WS in an EDBM stack containing ion-exchange and bipolar membranes. Conservation equations describing the fluid flow, mass-charge transport, and the second Wien effect are considered and solved using COMSOL Multiphysics software. Results from the computations are experimentally validated against data from an EDBM unit lab. Special emphasis is placed on the analysis of the concentration profiles, and the distribution of the electrical potential.

One of the most remarkable conclusions of this work is the comparison between electroneutrality and Poisson charge conservation approximations. Concentration profiles and electric potential distribution from electroneutrality and Poisson for the 1D model overlap. Electroneutrality should be conserved in all regions except from the Debye length (nano-meter scale); this work corroborates this statement. Based on this agreement between approximations, the electroneutrality approach is concluded to be valid to study the EDBM process in a more complex 2D geometry. Results from the simulations confirmed the selectivity of the membranes, and provided evidence of a considerable proton leakage to the adjacent channels; this is attributed to the different mobility values of the species. Moreover, the computations enable to examine the species transfer through the membranes and the presence of EDLs at the membrane-solution interfaces, which is caused by the polarization layer at the membranes and the electric field flowing through the stack. Additionally, the model presented in this work was able to capture the physics associated with the WS phenomena evidencing the water splitting reaction and the electrical perturbation at the BPMs junction. Finally, the model was satisfactorily validated against experimental data.

Although this model considered a short operation time and low voltage, the predicted trends reported in this work may be useful for developing EDBM models with more complex geometries, larger dimensions, geometries incorporating spacer's effect, water transport or even a three-dimensional geometry.

CRediT authorship contribution statement

T. León: Conceptualization, Methodology, Software, Validation, Formal analysis, Investigation, Writing – original draft, Visualization. **J. López:** Conceptualization, Methodology, Software, Validation, Formal analysis, Investigation, Writing – review & editing. **R. Torres:** Conceptualization, Software, Validation, Formal analysis, Investigation, Writing – review & editing. **J. Grau:** Conceptualization, Software, Validation, Investigation, Writing – review & editing. **L. Jofre:** Conceptualization, Software, Validation, Investigation, Resources, Formal analysis, Supervision, Writing – review & editing. **J.-L. Cortina:** Conceptualization, Validation, Resources, Supervision, Project administration, Funding acquisition, Writing – review & editing.

Declaration of competing interest

The authors declare that they have no known competing financial interests or personal relationships that could have appeared to influence the work reported in this paper.

Data availability

Data will be made available on request.

Acknowledgments

References

[1] T. Sokalski, A. Lewenstam, Application of Nernst±Planck and Poisson equations for interpretation of liquid-junction and membrane potentials in real-time and space domains, Electrochem. Commun. 3 (2001) 107–112. www.elsevier.nl/loca te/elecom.

[2] Y. Tanaka, Mass transport and energy consumption in ion-exchange membrane electrodialysis of seawater, J. Membr. Sci. 215 (2003) 265–279, https://doi.org/10.1016/S0376-7388(03)00020-6.

[3] E. Al-Dhubhani, R. Pärnamäe, J.W. Post, M. Saakes, M. Tedesco, Performance of five commercial bipolar membranes under forward and reverse bias conditions for acid-base flow battery applications, J. Membr. Sci. 640 (2021), https://doi.org/10.1016/j.memsci.2021.119748.

[4] S. Koter, Modeling of weak acid production by the EDB method, Separ. Purif. Technol. 57 (2007) 406–412, https://doi.org/10.1016/j.seppur.2006.03.005.

[5] M.P. Mier, R. Ibañez, I. Ortiz, Influence of ion concentration on the kinetics of electrodialysis with bipolar membranes, Separ. Purif. Technol. 59 (2008) 197–205, https://doi.org/10.1016/j.seppur.2007.06.015.

[6] S. Bunani, K. Yoshizuka, S. Nishihama, M. Arda, N. Kabay, Application of bipolar membrane electrodialysis (BMED) for simultaneous separation and recovery of boron and lithium from aqueous solutions, Desalination 424 (2017) 37–44, https://doi.org/10.1016/j.desal.2017.09.029.

[7] J.S. Tronc, F. Lamarche, J. Makhlouf, Effect of pH variation by electrodialysis on the inhibition of enzymatic browning in cloudy apple juice, J. Agric. Food Chem. 46 (1998) 829–833, https://doi.org/10.1021/jf970642e.

[8] M. Herrero-Gonzalez, P. Diaz-Guridi, A. Dominguez-Ramos, A. Irabien, R. Ibañez, Highly concentrated HCl and NaOH from brines using electrodialysis with bipolar membranes, Separ. Purif. Technol. 242 (2020), 116785, https://doi.org/10.1016/j.seppur.2020.116785.

[9] M. Reig, S. Casas, C. Valderrama, O. Gibert, J.L. Cortina, Integration of monopolar and bipolar electrodialysis for valorization of seawater reverse osmosis desalination brines: production of strong acid and base, Desalination 398 (2016) 87–97, https://doi.org/10.1016/j.desal.2016.07.024.

[10] C. Huang, T. Xu, Y. Zhang, Y. Xue, G. Chen, Application of electrodialysis to the production of organic acids: state-of-the-art and recent developments, J. Membr. Sci. 288 (2007) 1–12, https://doi.org/10.1016/j.memsci.2006.11.026.

[11] R. Ibáñez, A. Pérez-González, P. Gómez, A.M. Urtiaga, I. Ortiz, Acid and base recovery from softened reverse osmosis (RO) brines. Experimental assessment using model concentrates, Desalination 309 (2013) 165–170, https://doi.org/10.1016/j.desal.2012.10.006.

[12] A. Culcasi, L. Gurreri, A. Cipollina, A. Tamburini, G. Micale, A comprehensive multi-scale model for bipolar membrane electrodialysis (BMED), Chem. Eng. J. 437 (2022), 135317, https://doi.org/10.1016/j.cej.2022.135317.

[13] M. La Cerva, L. Gurreri, M. Tedesco, A. Cipollina, M. Ciofalo, A. Tamburini, G. Micale, Determination of limiting current density and current efficiency in electrodialysis units, Desalination 445 (2018) 138–148, https://doi.org/10.1016/j.desal.2018.07.028.

[14] A. Culcasi, L. Gurreri, A. Zaffora, A. Cosenza, A. Tamburini, G. Micale, On the modelling of an Acid/Base Flow Battery: an innovative electrical energy storage device based on pH and salinity gradients, Appl. Energy 277 (2020), 115576, https://doi.org/10.1016/j.apenergy.2020.115576.

[15] A.V. Kovalenko, M. Wessling, V.V. Nikonenko, S.A. Mareev, I.A. Moroz, E. Evdochenko, M.K. Urtenov, Space-Charge breakdown phenomenon and spatio-temporal ion concentration and fluid flow patterns in overlimiting current electrodialysis, J. Membr. Sci. 636 (2021), 119583, https://doi.org/10.1016/j.memsci.2021.119583.

[16] M.M. Generous, N.A.A. Qasem, S.M. Zubair, The significance of modeling electrodialysis desalination using multi-component saline water, Desalination 496 (2020), 114347, https://doi.org/10.1016/j.desal.2020.114347.

[17] P. Moon, G. Sandí, D. Stevens, R. Kizilel, Computational modeling of ionic transport in continuous and batch electrodialysis, Separ. Sci. Technol. 39 (2004) 2531–2555, https://doi.org/10.1081/SS-200026714.

[18] S.A. Mareev, E. Evdochenko, M. Wessling, O.A. Kozaderova, S.I. Niftaliev, N. D. Pismenskaya, V.V. Nikonenko, A comprehensive mathematical model of water splitting in bipolar membranes: impact of the spatial distribution of fixed charges and catalyst at bipolar junction, J. Membr. Sci. 603 (2020), 118010, https://doi.org/10.1016/j.memsci.2020.118010.

[19] Kuldeep, P. Kauranen, H. Pajari, R. Pajarre, L. Murtomäki, Electrodiffusion of ions in ion exchange membranes: finite element simulations and experiments, Chem. Eng. J. Adv. 8 (2021), https://doi.org/10.1016/j.ceja.2021.100169.

[20] V.I. Zabolotsky, L. Novak, A.V. Kovalenko, V.V. Nikonenko, M.H. Urtenov, K. A. Lebedev, A.Y. But, Electroconvection in systems with heterogeneous ion-exchange membranes, Petrol. Chem. 57 (2017) 779–789, https://doi.org/10.1134/S0965544117090109.

[21] E.J.F. Dickinson, H. Ekström, E. Fontes, COMSOL Multiphysics®: finite element software for electrochemical analysis. A mini-review, Electrochem. Commun. 40 (2014) 71–74, https://doi.org/10.1016/j.elecom.2013.12.020.

[22] V. Nikonenko, M. Urtenov, S. Mareev, G. Pourcelly, Mathematical modeling of the effect of water splitting on ion transfer in the depleted diffusion layer near an ion-exchange membrane, Membranes (Basel) 10 (2020), https://doi.org/10.3390/membranes10020022.

[23] T. Aritomi, T. van den Boomgaard, H. Strathmann, Current-voltage curve of a bipolar membrane at high current density, Desalination 104 (1996) 13–18, https://doi.org/10.1016/0011-9164(96)00021-5.

[24] R. Pärnamäe, S. Mareev, V. Nikonenko, S. Melnikov, N. Sheldeshov, V. Zabolotskii, H.V.M. Hamelers, M. Tedesco, Bipolar membranes: a review on principles, latest developments, and applications, J. Membr. Sci. 617 (2021), https://doi.org/10.1016/j.memsci.2020.118538.

[25] H. Strathmann, J.J. Krol, H.J. Rapp, G. Eigenberger, Limiting current density and water dissociation in bipolar membranes, J. Membr. Sci. 125 (1997) 123–142, https://doi.org/10.1016/S0376-7388(96)00185-8.

[26] Y. Tanaka, Water dissociation reaction generated in an ion exchange membrane, J. Membr. Sci. 350 (2010) 347–360, https://doi.org/10.1016/j.memsci.2010.01.010.

[27] R. Simons, Electric field effects on proton transfer between ionizable groups and water in ion exchange membranes, Electrochim. Acta 29 (1984) 151–158, https://doi.org/10.1016/0013-4686(84)87040-1.

[28] Z. Zourmand, F. Faridirad, N. Kasiri, T. Mohammadi, Mass transfer modeling of desalination through an electrodialysis cell, Desalination 359 (2015) 41–51, https://doi.org/10.1016/j.desal.2014.12.008.

[29] F. White, Mecanica de fluidos 5ta E, in: Mec. Fluidos, Fith Editi, McGrawHill, 2006, pp. 219–287. https://www.academia.edu/35477659/Mecanica_de_los_Fluidos_White_5ta_Edición.

[30] T. Solomon, The definition and unit of ionic strength, J. Chem. Educ. 78 (2001) 1691, https://doi.org/10.1021/ed078p1691.

[31] L. Onsager, Deviations from Ohm's law in weak electrolytes, J. Chem. Phys. 2 (1934) 599–615, https://doi.org/10.1063/1.1749541.

[32] G.S. Trivedi, B.G. Shah, S.K. Adhikary, V.K. Indusekhar, R. Rangarajan, Studies on bipolar membranes, React. Funct. Polym. 28 (1996) 243–251, https://doi.org/10.1016/1381-5148(95)00088-7.

[33] L. Gurreri, G. Battaglia, A. Tamburini, A. Cipollina, G. Micale, M. Ciofalo, Multi-physical modelling of reverse electrodialysis, Desalination 423 (2017) 52–64, https://doi.org/10.1016/j.desal.2017.09.006.

[34] T. Preney, J.D. Wheeler, P. Namy, Adaptive Mesh Refinement : Quantitative Computation of a Rising Bubble Using COMSOL Multiphysics, COMSOL Conf, 2016.

[35] R. Kodým, D. Šnita, K. Bouzek, Mathematical modeling of electromembrane processes, in: Curr. Trends Futur. Dev. Membr. Membr. Desalin. Syst. Next Gener., 2019, pp. 285–326, https://doi.org/10.1016/B978-0-12-813551-8.00012-7.

[36] Y. Wang, X. Zhang, T. Xu, Integration of conventional electrodialysis and electrodialysis with bipolar membranes for production of organic acids, J. Membr. Sci. 365 (2010) 294–301, https://doi.org/10.1016/j.memsci.2010.09.018.

[37] H.J. Lee, F. Sarfert, H. Strathmann, S.H. Moon, Designing of an electrodialysis desalination plant, Desalination 142 (2002) 267–286, https://doi.org/10.1016/S0011-9164(02)00208-4.

[38] W.T. Grubb, Ionic migration in ion-exchange membranes, J. Phys. Chem. 63 (1959) 55–58, https://doi.org/10.1021/j150571a015.

[39] E.J.F. Dickinson, J.G. Limon-Petersen, R.G. Compton, The electroneutrality approximation in electrochemistry, J. Solid State Electrochem. 15 (2011) 1335–1345, https://doi.org/10.1007/s10008-011-1323-X.

[40] M. Pabst, Analytical solution of the Poisson-Nernst-Planck equations for an electrochemical system close to electroneutrality, J. Chem. Phys. 140 (2014), https://doi.org/10.1063/1.4881599.

[41] V.M. Volgin, A.D. Davydov, Ionic transport through ion-exchange and bipolar membranes, J. Membr. Sci. 259 (2005) 110–121, https://doi.org/10.1016/j.memsci.2005.03.010.

[42] P. Ramírez, H.J. Rapp, S. Reichle, H. Strathmann, S. Mafé, Current-voltage curves of bipolar membranes, J. Appl. Phys. 72 (1992) 259–264, https://doi.org/10.1063/1.352124.

[43] N.W. Ryan, M.M. Johnson, Transistion from laminar to turbulent flow in pipes, AIChE J. 5 (1959) 433–435, https://doi.org/10.1002/aic.690050407.

[44] N. Agmon, Mechanism of hydroxide mobility, Chem. Phys. Lett. 319 (2000) 247–252, https://doi.org/10.1016/S0009-2614(00)00136-6.

[45] J. Ran, L. Wu, Y. He, Z. Yang, Y. Wang, C. Jiang, L. Ge, E. Bakangura, T. Xu, Ion exchange membranes: new developments and applications, J. Membr. Sci. 522 (2017) 267–291, https://doi.org/10.1016/j.memsci.2016.09.033.

[46] Y. Lorrain, G. Pourcelly, C. Gavach, Influence of cations on the proton leakage through anion-exchange membranes, J. Membr. Sci. 110 (1996) 181–190, https://doi.org/10.1016/0376-7388(95)00246-4.

[47] D. Raucq, G. Pourcelly, C. Gavach, Production of sulphuric acid and caustic soda from sodium sulphate by electromembrane processes. Comparison between electro-electrodialysis and electrodialysis on bipolar membrane, Desalination 91 (1993) 163–175, https://doi.org/10.1016/0011-9164(93)80055-R.

[48] W. Schmickler, Electrochemical Theory: Double Layer, Elsevier Inc., 2014, https://doi.org/10.1016/b978-0-12-409547-2.11149-7.

[49] D.A. Vermaas, S. Wiegman, T. Nagaki, W.A. Smith, Ion transport mechanisms in bipolar membranes for (photo)electrochemical water splitting, Sustain. Energy Fuels 2 (2018) 2006–2015, https://doi.org/10.1039/c8se00118a.

[50] A. Ortega, L.F. Arenas, J.J.H. Pijpers, D.L. Vicencio, J.C. Martínez, F.A. Rodríguez, E.P. Rivero, Modelling water dissociation, acid-base neutralization and ion transport in bipolar membranes for acid-base flow batteries, J. Membr. Sci. 641 (2022), 119899, https://doi.org/10.1016/j.memsci.2021.119899.

[51] J. Wiśniewski, G. Wiśniewska, T. Winnicki, Application of bipolar electrodialysis to the recovery of acids and bases from water solutions, Desalination 169 (2004) 11–20, https://doi.org/10.1016/j.desal.2004.08.003.

[52] K. Nagasubramanian, F.P. Chlanda, K.J. Liu, Use of bipolar membranes for generation of acid and base - an engineering and economic analysis, J. Membr. Sci. 2 (1977) 109–124, https://doi.org/10.1016/S0376-7388(00)83237-8.